ELSEVIER

Journal of Molecular Structure (Theochem) 506 (2000) 55–70

THEO CHEM

www.elsevier.nl/locate/theochem

Local regularity and non-recrossing path in transition state—a new strategy in chemical reaction theories ☆

T. Komatsuzaki*, R.S. Berry

Department of Chemistry, The University of Chicago, Chicago, IL 60637, USA

Abstract

We analyze local regularities in the regions of transition states of a 6-atom Lennard-Jones cluster to demonstrate how one can choose a non-recrossing reaction path in phase space along which the transmission coefficient for the classical reaction path is unity from threshold up to a moderately high energy, above which the transition state is chaotic, and how one can picture the nonlinear, full-phase-space character of the dividing hypersurface by projecting it into spaces of only a few dimensions. These overcome one of the long-standing ambiguities in chemical reaction theories, the recrossing problem, up to moderately high energies, and make transition state theory more generalized, applicable even in cases in which apparent recrossings spoil the conventional theory.

Keywords: Isomerization reaction dynamics; Regular and chaotic motion in transition states; Multi-dimensional phase-space dividing surface; Six-atom argon cluster; Lie canonical perturbation theory

1. Introduction

A comprehensive understanding of how a chemical species finds a reaction path to cross through a transition state from a reactant state to a product state is one of the most intriguing subjects in chemistry and biology [1–8]. Conventional (classical) transition state theories (TST) [1–3] assume that the reaction system begins with quasi-equilibrium between the reactant state and systems crossing the transition state in the products direction. The trajectories of the activated reaction system pass through a hypersurface that divides space into reactant and product regions. Systems crossing that surface in the product direction will not reach it again before being captured into a product state. One of the frequently observed discrepancies between the TST rate coefficient and its experimental counterpart, especially for systems with many degrees of freedom (DOF), comes from the violation of that no-recrossing assumption [4]. Kramers [5], and Grote and Hynes [4] have proposed other types of rate theories, based on Langevin and generalized Langevin formalism: these can take into account barrier recrossings, in which one chosen reactive degree of freedom moves under a friction and a random force from the other nonreactive degrees of freedom. Most widely used reaction coordinates and dividing surfaces are defined in configurational space. Davis and Gray [9] first showed that in Hamiltonian systems with only two DOF, the transition state defined as the separatrix in the phase space is always free from barrier recrossings, so the transmission coefficient for such systems is unity. Their inference depends crucially on the Poincaré section having only

☆ Presented at the 5th World Congress of Theoretically Oriented Chemists (WATOC), Imperial College, London, 1–6 August, 1999.

* Corresponding author. Present address: Department of Earth and Planetary Sciences, Faculty of Science, Kobe University, Nada, Kobe 657-8501, Japan.

0166-1280/00/$ - see front matter
PII: S0166-1280(00)00402-4

two dimensions; No general theory exists yet for systems of higher dimensionality [10–13]. Several recent, remarkable theoretical [14–23] and experimental [24–26] developments have revealed that during passage through the transition state the system's trajectories become collimated and more regularized than those in the potential well, i.e. they develop an approximate *local* invariant of motion at energies just above that of the transition state, even though the dynamics in the potential well is fully chaotic under these conditions. It was also shown that at higher energies above the threshold, emerging mode–mode mixings wipe out almost all invariants of motion even in the region of the transition state.

Recently, we have developed a new method to look more deeply into these local regularities associated with the transition state of *N*-particle Hamiltonian systems [27–30]. The crux of the method is the application of Lie canonical perturbation theory (LCPT) [31–35] to a region around a saddle point. This theory constructs a nonlinear transformation to a hyperbolic coordinate system, which "rotates away" the recrossings and non-regular behavior, especially of the motion along the reaction coordinate. In this paper, we use a simple cluster of six atoms bound by pairwise Lennard-Jones potentials to show that, even into the high-energy region in which the transition state becomes manifestly chaotic, at least one action, that associated with the reaction coordinate, remains an approximate invariant of motion over the region of the transition state. Furthermore, it is possible to choose a multi-dimensional phase-space dividing surface through which the transmission coefficient for the classical reaction path is unity. We visualize this dividing hypersurface in the phase space with projections onto a subspace of a few principal coordinates. This device reveals how the "shape" of the reaction bottleneck depends on the energy of the system and how a system makes its complicated passage through its saddles.

2. Theory [29,30]

We first expand the full 3*N*-DOF potential energy surface about a chosen stationary point, i.e. a minimum, simple saddle, or higher-rank saddle. We construct the zeroth-order Hamiltonian as a set of harmonic oscillators, which might include some negatively curved modes, i.e. reactive modes. Then we establish the higher-order perturbation terms consisting of nonlinear couplings expressed in arbitrary combinations of coordinates.

$$H = H_0 + \sum_{n=1}^{\infty} \epsilon^n H_n \tag{1}$$

where

$$H_0(\mathbf{p},\mathbf{q}) = \tfrac{1}{2}\sum_j (p_j^2 + \omega_j^2 q_j^2) = \sum_{j=1} \omega_j J_j = H_0(\mathbf{J}) \tag{2}$$

$$\sum_{n=1}^{\infty} \epsilon^n H_n(\mathbf{p},\mathbf{q}) = \epsilon \sum_{j,k,l} C_{jkl} q_j q_k q_l \tag{3}$$

$$+\epsilon^2 \sum_{j,k,l,m} C_{jklm} q_j q_k q_l q_m + \cdots = \sum_{n=1} \epsilon^n H_n(\mathbf{J},\boldsymbol{\Theta}) \tag{4}$$

Here q_j and p_j are the jth normal coordinate and its conjugate momentum, respectively; ω_j and $C_{jkl}, C_{jklm}, \ldots$ are, respectively, the frequency of the jth mode, the third-order coupling coefficients among q_j, q_k, and q_l and the fourth-order coupling coefficients among q_j, q_k, q_l, and q_m, and so forth. $\mathbf{J}$ and $\boldsymbol{\Theta}$ are, respectively, action and the conjugate angle variables of H_0, and ϵ is the strength of the perturbation. The frequency associated with any unstable reactive mode F are pure-imaginary; those of stable modes are of course real. In this paper, we focus on a $(3N-6)$-DOF Hamiltonian system around a first-rank saddle with total linear and angular momenta of zero. To begin, we eliminate the six degrees of freedom of the total translational and rotational motions [36]. We apply Lie canonical perturbation theory (LCPT) to the regional Hamiltonians obtained by the expansion around the stationary point.

Based on Lie transforms, LCPT [31–35] canonically transforms $(\mathbf{p},\mathbf{q})$ to a new $(\bar{\mathbf{p}},\bar{\mathbf{q}})$ coordinate system so as to make the new Hamiltonian $\bar{H}(\bar{\mathbf{p}},\bar{\mathbf{q}})$ as close to integrable as possible: this generates as simple a form as possible by eliminating its dependencies on the new angle variables $\bar{\boldsymbol{\Theta}}$.

$$\bar{H}(\bar{\mathbf{p}},\bar{\mathbf{q}}) = \bar{H}(\bar{\mathbf{J}},\bar{\boldsymbol{\Theta}}) = \bar{H}(\bar{\mathbf{J}}) = \sum_{n=0} \epsilon^n \bar{H}_n(\bar{\mathbf{J}}) \tag{5}$$

If such exists (at the order of the perturbative calculation being performed), the $\bar{H}$ has the following dynamical properties [27–30]: the new action and angle

variables for the kth mode are expressed as

$$\frac{\mathrm{d}\bar{J}_k}{\mathrm{d}t} = \dot{\bar{J}}_k = -\frac{\partial \bar{H}(\bar{\mathbf{J}})}{\partial \bar{\Theta}_k} = 0 \tag{6}$$

$$\bar{J}_k = \text{constant} \qquad (k = 1, 2, 3, \ldots, 3N-6), \tag{7}$$

and

$$\dot{\bar{\Theta}}_k = \frac{\partial \bar{H}(\bar{\mathbf{J}})}{\partial \bar{J}_k} \equiv \bar{\omega}_k(\bar{\mathbf{J}}) = \text{constant} \tag{8}$$

$$\bar{\Theta}_k = \bar{\omega}_k(\bar{\mathbf{J}})t + \beta_k \tag{9}$$

where β_k is the arbitrary initial phase factor of the kth mode. From there, the equations of motion with respect to the new coordinates $\bar{\mathbf{q}}$ and momenta $\bar{\mathbf{p}}$ are obtained from the Hamiltonian equations of motion obeying $\bar{H}$;

$$\frac{\mathrm{d}^2\bar{q}_k(\mathbf{p},\mathbf{q})}{\mathrm{d}t^2} + \bar{\omega}_k^2\bar{q}_k(\mathbf{p},\mathbf{q}) = 0 \tag{10}$$

and

$$\bar{p}_k(\mathbf{p},\mathbf{q}) = \frac{\omega_k}{\bar{\omega}_k}\frac{\mathrm{d}\bar{q}_k(\mathbf{p},\mathbf{q})}{\mathrm{d}t} \tag{11}$$

where $\bar{\omega}_k(=\bar{\omega}_k(\bar{\mathbf{J}}) = \bar{\omega}_k(\bar{\mathbf{p}},\bar{\mathbf{q}}))$ is independent of time t because the $\bar{\mathbf{J}}$ are constant through all t (Eq. (6)). In general, new transformed physical quantities $\bar{A}$, e.g. a new Hamiltonian $\bar{H}$, and new action $\bar{J}_k$, frequency $\bar{\omega}_k$, momentum $\bar{p}_k$, and coordinate $\bar{q}_k$ of the kth mode, can be represented in terms of the original $\mathbf{p}$ and $\mathbf{q}$.

$$\bar{A}^{i\text{th}} = \bar{A}^{i\text{th}}(\mathbf{p},\mathbf{q}) = \sum_{n=0}^{i}\epsilon^n\bar{A}_n(\mathbf{p},\mathbf{q}) \tag{12}$$

The $\bar{p}_k(\mathbf{p},\mathbf{q})$ and $\bar{q}_k(\mathbf{p},\mathbf{q})$ have the following forms, respectively

$$\bar{p}_k(\mathbf{p},\mathbf{q}) = \sum_j c_j\mathbf{p}^{2n-1}\mathbf{q}^m \tag{13}$$

$$\bar{q}_k(\mathbf{p},\mathbf{q}) = \sum_j d_j\mathbf{p}^{2n}\mathbf{q}^m \tag{14}$$

where c_j and d_j denote the coefficient of the jth term, n, $m(\geq 0)$ are arbitrary integers, and

$$\mathbf{q}^m = q_1^{m_1}q_2^{m_2}q_3^{m_3}\cdots q_{3N-6}^{m_{3N-6}} \qquad \left(\sum_{j=1}^{3N-6} m_j = m\right)$$

etc. The new $\bar{p}_k(\mathbf{p},\mathbf{q})$ and $\bar{q}_k(\mathbf{p},\mathbf{q})$ maintain time reversibility. The contributions of the original p_k and q_k in $\bar{p}_k^{i\text{th}}(\mathbf{p},\mathbf{q})$ and $\bar{q}_k^{i\text{th}}(\mathbf{p},\mathbf{q})$ are not necessarily large and almost all modes contribute to $\bar{p}_k^{i\text{th}}$ and $\bar{q}_k^{i\text{th}}$ for $i \geq 1$ [29].

It would be quite remarkable to be able to make the $\bar{J}_k$s constant, because Eqs. (10) and (11) tell us that even though the motions look quite complicated in the old coordinate system, it would be possible to reformulate them into simple decoupled periodic orbits in the phase space. This would mean that by knowing the solution of the equation of motion a priori, we would have no need to do trajectory calculations. But we inevitably ask "is this true?"

There exists a well-known obstacle in proceeding any canonical perturbative calculation, so-called "small-denominator problem" [31]. Almost all the coefficients appearing in the successive terms c_j and d_j, etc. have in their denominators an integer linear combination of fundamental frequencies $\sum_{k=1}^{3N-6} n_k\omega_k$ (where n_k is arbitrary integer). The problem would arise in cases in which the combination vanishes identically at some order ϵ^n of the perturbative calculation:

$$\sum_{k=1}^{3N-6} n_k\omega_k \leq \mathrm{O}(\epsilon^n) \tag{15}$$

which would make such a perturbative calculation diverge. If the system exhibits this small-denominator problem, or, in other terms, a (near-)commensurable condition, the new Hamiltonian probably cannot be represented as a function of constant actions only. That is, no invariants of action can be anticipated through a region in question; instead the perturbative calculation would have to be performed to infinite order or the new Hamiltonian would include the corresponding angle variables to avoid the divergence [33–35].

It is quite likely that in many-dimensional systems, those near-commensurable conditions densely distribute in typical regions throughout the phase space, and hence Eqs. (10) and (11) would become meaningless there. This is a reason why such canonical perturbation theories have been rarely used for exploring dynamics of *many-degrees-of-freedom* chemical systems. However the non-uniform nature of dynamical properties of inert gas atomic clusters [14–21] and

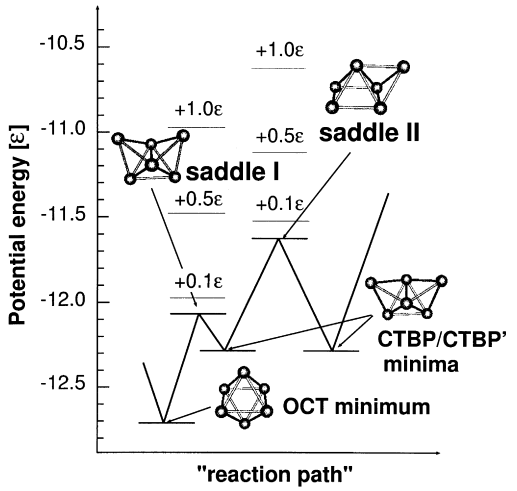

Fig. 1. A schematical picture of the potential energy surface of Ar_6. CTBP′ is a permutational isomer of the CTBP minimum neighboring on the OCT minimum.

the quantized thresholds in the transition states observed in experiments with some systems [24–26,37–39] imply that some but not all invariants of motion are more likely to survive in the vicinity of (at least first-rank) saddle points than in regions around stable reactant and product states. LCPT is then, still powerful enough to reveal such invariancies. Rather, the method provides us with a new phase-space dividing surface free from recrossing up to moderately high energy.

3. Calculations

We apply this method to saddle crossing dynamics in Ar_6, whose interactions are represented by the sum of pairwise Lennard-Jones potentials

$$V(\mathbf{r}) = 4\epsilon \sum_{i>j}^{N,N} \left[\left(\frac{\sigma}{r_{ij}} \right)^{12} - \left(\frac{\sigma}{r_{ij}} \right)^{6} \right] \tag{16}$$

We assign laboratory scales of energy and length appropriate for argon [29] and the total linear and angular momenta are set to zero. The potential energy profile is shown in Fig. 1. The Ar_6 cluster has only two geometrically distinct kinds of potential energy minima, the octahedral (OCT) global minimum with energy $E = -12.712\epsilon$, and the other, higher capped trigonal bipyramid (CTBP) minimum with energy $E = -12.303\epsilon$. There are two distinct kinds of first-rank saddles. One saddle (saddle I) at energy $E = -12.079\epsilon$ joins the OCT and the CTBP minima, and the other higher saddle (saddle II) at energy $E = -11.630\epsilon$ joins two permutationally distinct CTBP structures, in a local topography slightly flatter than the lower saddle. The computational recipe for constructing the $3N - 6(= 12)$-DOF regional Hamiltonian was described elsewhere [29]. The regional Hamiltonians are composed of the zeroth-order quadratic diagonal coordinate and momentum terms and 106 three-body, and 365 four-body couplings terms for saddle I, and 189 and 674 for saddle II. Throughout this paper the parabolic barrier coordinate F in the original $(\mathbf{p},\mathbf{q})$ space is denoted as q_1 and in the new $(\bar{\mathbf{p}}, \bar{\mathbf{q}})$ space as $\bar{q}_1$; the other bath coordinates for the old (new) spaces are written as $q_2, q_3, \ldots, q_{12}$ $(\bar{q}_2, \bar{q}_3, \ldots, \bar{q}_{12})$ in order of increasing frequencies, so that $\omega_2 \le \omega_3 \le \cdots \le \omega_{12}$ $(\bar{\omega}_2 \le \bar{\omega}_3 \le \cdots \le \bar{\omega}_{12})$. The units of energy, coordinate, momentum, action, frequency, temperature, mass and time are ϵ, $m^{1/2}\sigma$, $m^{1/2}\sigma\,\mathrm{ps}^{-1}$, K ps, ps^{-1}, K, argon atomic mass ($m =$ 39.948 amu) and ps, unless otherwise noted.

The trajectories from a minimum rarely cross the energy barrier at an energy very much higher than E/f where E and f are the total energy of the system and the number of DOF, respectively. Hence for analyses of the infrequent saddle crossings, we employed a modified Keck–Anderson method [30] to generate the microcanonical ensemble in the saddle regions; in this study 10,000 "well–saddle–well" trajectories, which are found to be enough to yield statistical convergence in calculating the transmission coefficients in terms of a new dividing hypersurface $S(\bar{q}_1^{\,i\text{th}}(\mathbf{p},\mathbf{q}) = 0)$ for $i = 0$, 1, 2 at 0.1, 0.5, and 1.0ϵ above each saddle point energy. For the trajectory calculations we used a fourth-order Runge–Kutta method with adaptive step-size control [40], which dynamically adjusts the step size to reduce the error of integration in calculation. The total energies in our MD calculations were conserved within $\pm 1 \times 10^{-6}\epsilon$.

By monitoring the new action $\bar{J}_k(\mathbf{p},\mathbf{q})$ and the frequency $\bar{\omega}_k(\mathbf{p},\mathbf{q})$ at several total energies above each saddle point energy, we show here that in the transition region, those quantities associated with a reactive mode F exhibit near-constancy of motion up to a moderately high energy in dynamics obeying

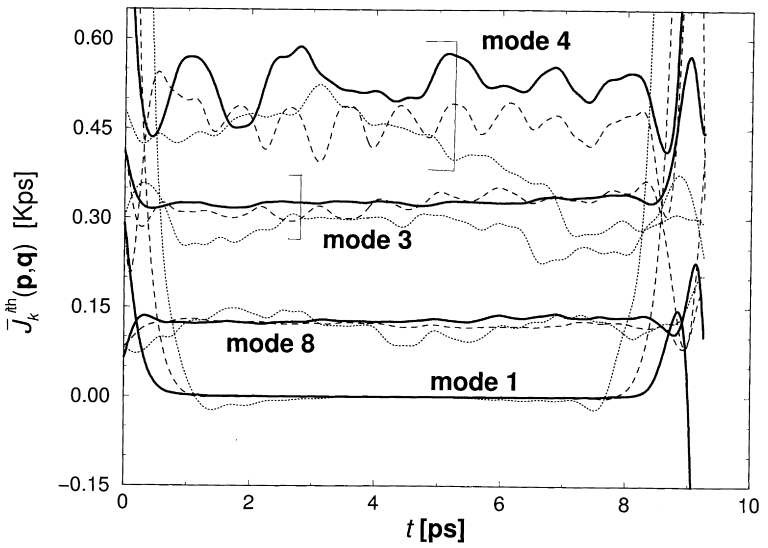

Fig. 2. The time dependencies of $\bar{J}_k(\mathbf{p},\mathbf{q})$ ($k = 1, 3, 4, 8$) for a representative saddle-crossing trajectory at 0.05ϵ. The units of action for mode 1 must be multiplied by a factor of an imaginary number *i*. The dash-dot, dash, and bold-solid lines denote the zeroth-, first-, and second-order actions, respectively.

equations of motion of the *original* Hamiltonian $H(\mathbf{p},\mathbf{q})$. Moreover the dividing hypersurface, defined by the condition that the reactive coordinate in the transformed coordinates is zero there, $S(\bar{q}_1^{ith}(\mathbf{p},\mathbf{q}) = 0)$, is almost free from recrossings.

4. Results and discussion

4.1. Invariancies of actions in a region of transition state

First, we look into the new action variables $\bar{J}_k(\mathbf{p},\mathbf{q})$ along two representative "well–saddle–well" trajectories obeying the original Hamiltonian $H(\mathbf{p},\mathbf{q})$ at $E = 0.05\epsilon$, and 0.5ϵ over saddle I. Even at $E = 0.05\epsilon$, only slightly above the saddle point energy; just 8% of the activation energy 0.633ϵ from the OCT minimum, almost of all the zeroth-order actions $\bar{J}^{0th}(\mathbf{p},\mathbf{q})$ do not maintain constancy of motion at all; i.e. even there, most modes violate a simple normal mode picture. As an example, Fig. 2 shows the zeroth, first, and second order $\bar{J}_k(t)$ for $k = 1$, 3, 4, and 8. This figure shows that the higher the order to which the LCPT is carried, the more *some* of the actions $\bar{J}_k$ tend to be well conserved, and to persist as nearly-conserved quantities for longer time periods. Second-order LCPT can extract "good" invariants of motion associated with the modes $\bar{q}_1^{2nd}$, $\bar{q}_3^{2nd}$, and $\bar{q}_8^{2nd}$ in the saddle region. On the other hand for mode 4, although LCPT seemingly improves the constancy of $\bar{J}_4(\mathbf{p},\mathbf{q})$ in the zeroth-order estimate, the second-order LCPT does not yield a good invariant of motion for this mode, compared with modes 1, 3, and 8. The initial drop and/or rise observed in the $\bar{J}_k(\mathbf{p},\mathbf{q})$ at short times (e.g. 0–0.5 ps in Fig. 2) to the flat region implies that initially, the system is just entering a "regular region" near the saddle point, outside of which the system is subject to considerable nonlinearities of the PES; in that region away from the saddle, we can expect to find no approximate invariant of motion at any given finite order of LCPT. This implies (at least for the sampled trajectory at second-order) that in the saddle region, some modes are well decoupled and follow periodic orbits in phase space; examples are those of Eqs. (10) and (11), while the others are coupled at least within coupled-mode-subsets in the $(\bar{\mathbf{p}}^{2nd}, \bar{\mathbf{q}}^{2nd})$ coordinate system. However away from the saddle, anharmonicity and mode-mode coupling remove any possibility of "regional" approximate constants of motion.

How does the crossing dynamics change as the

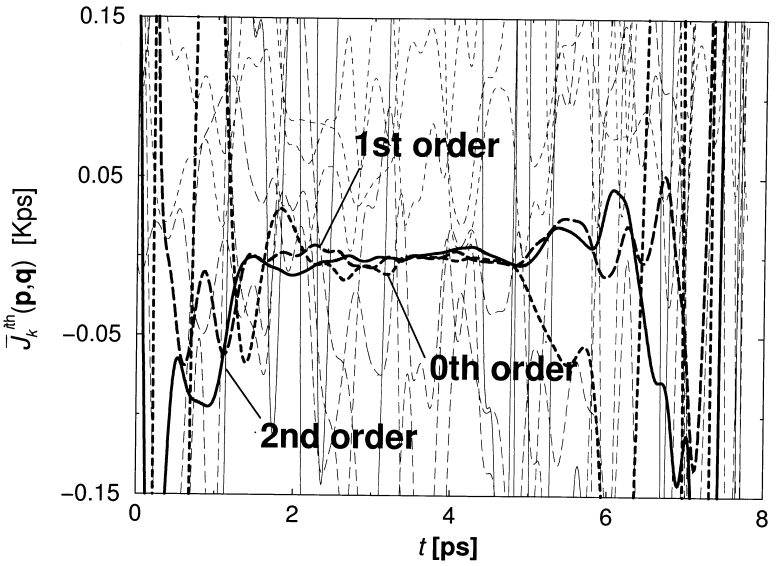

Fig. 3. The action $\bar{J}_k(\mathbf{p},\mathbf{q})$ at 0.5ϵ for a representative saddle-crossing trajectory at 0.5ϵ. The dash-dot, dash, and solid lines denote the zeroth-, first-, and second-order actions. The actions of mode 1 are emphasized by the bold-lines.

energy of the system increases? Intuition suggests that at higher total energies, the nonlinearities of the PES cannot be considered as a "sufficiently weak perturbation," and the number of approximate local invariants of motion becomes smaller and smaller, going to zero at sufficiently high energy. Consequently the local crossing dynamics should change from quasi-regular to chaotic, with increasing energy. This is actually a universal picture with chaotic dynamics in the vicinity of potential energy minima, especially for many-DOF chemical systems, which validates the assumption of local vibrational equilibrium in the reactant well. Fig. 3 at $E = 0.5\epsilon$, 79% above of the activation energy from the OCT minimum, shows that *while none of the action variables for the bath modes,* $\bar{q}_k$ $(k = 2,3,\ldots,3N-6)$, *are conserved even through second order of LCPT, the one variable that stands out among all the rest is the reaction coordinate* $\bar{q}_1$, *whose action becomes more well-conserved as the LCPT order increases.*

4.2. Recrossing trajectories in the new coordinate system

Next, how do these saddle-crossing trajectories look in the $(\bar{\mathbf{p}},\bar{\mathbf{q}})$ space? The projections of the "recrossing" trajectories at $E = 0.05$, and 0.5ϵ at saddle I onto the zeroth, first, and second order new coordinate plane of $\bar{q}_j(\mathbf{p},\mathbf{q})$ and $\bar{q}_k(\mathbf{p},\mathbf{q})$ are shown in Figs. 4 and 5. Here the zeroth-order coordinate system $(\bar{\mathbf{p}}^{0th},\bar{\mathbf{q}}^{0th})$ is the original **(p,q)** system we have used to describe the cluster.

First let us examine the projections onto a two-dimensional subspace chosen from the bath degrees of freedom, $(\bar{q}_3^{ith}(\mathbf{p},\mathbf{q}),\bar{q}_8^{ith}(\mathbf{p},\mathbf{q}))$, at both the energies. At the lower energy, 0.05ϵ, (see Fig. 4a), in all the orders one can see the approximate Lissajous figures, which implies that in the subspace of these two bath degrees of freedom, the motions are composed of two approximately decoupled, simple harmonic oscillations. As the total energy increases to ten times higher, ca. 0.5ϵ, as one may anticipate from Fig. 3, no approximate invariants of motion survive in the bath DOF. Between 0.05ϵ and 0.5ϵ, the bath motions change topologically from regular to fully chaotic (see Fig. 4b).

An even more striking consequence of the LCPT transformation appears in the behavior of the reactive degrees of freedom. Fig. 5 shows the projections of the recrossing trajectories onto the $(\bar{q}_1^{ith}(\mathbf{p},\mathrm{q}),\bar{\mathbf{q}}_4^{ith}(\mathbf{p},\mathbf{q}))$. The abscissas in the figure correspond to a reaction coordinate, i.e. $\bar{\omega}_1 \in \Im$, and the ordinates, to the bath

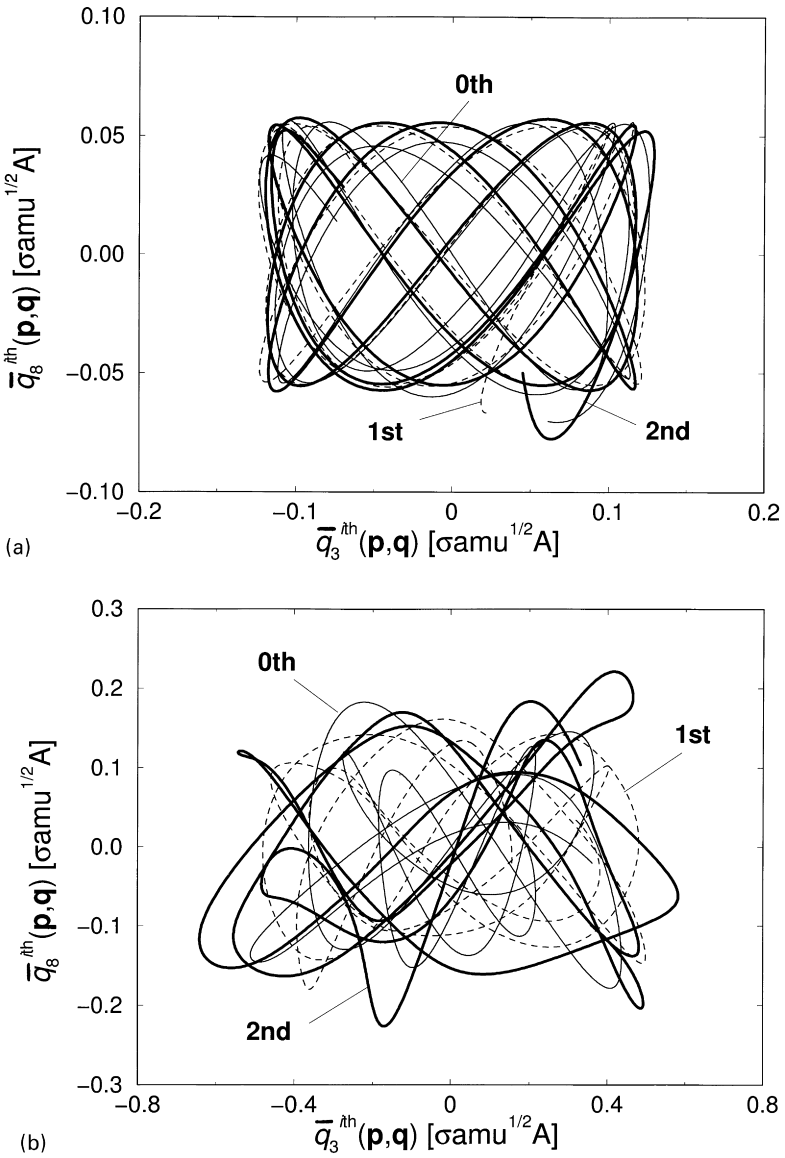

Fig. 4. The projections of the recrossing trajectories onto the zeroth-, first-, and second-order ($\bar{q}_3(\mathbf{p},\mathbf{q})$, $\bar{q}_8(\mathbf{p},\mathbf{q})$) plane: (a) at 0.05ϵ in Fig. 2; and (b) at 0.5ϵ in Fig. 3.

coordinates, i.e. $\bar{\omega}_4 \in \Re$, in each order coordinate system. To do this, we first examine the non-reactive recrossing trajectory at 0.05ϵ (see Fig. 5a), the non-reactive recrossing motion over the naive dividing surface $S(q_1 = 0)$. In first and second orders, this trajectory never crosses any dividing surface $S(\bar{q}_1^{1st}(\mathbf{p},\mathbf{q}) = 0)$ and $S(\bar{q}_1^{2nd}(\mathbf{p},\mathbf{q}) = 0)$ from the CTBP minimum where the trajectory originates. The trajectory is simply not that of a reaction. We can deduce one important feature from this figure: if local invariants of motion associated with the higher-order reactive LCPT coordinate, e.g. $\bar{q}_1^{2nd}$, exist, any non-reactive recrossing trajectories observed over the naive dividing surface $S(q_1 = 0)$ transform to trajectories that do not cross the LCPT dividing surface, $S(\bar{q}_1^{2nd}(\mathbf{p},\mathbf{q}) = 0)$, in higher orders of

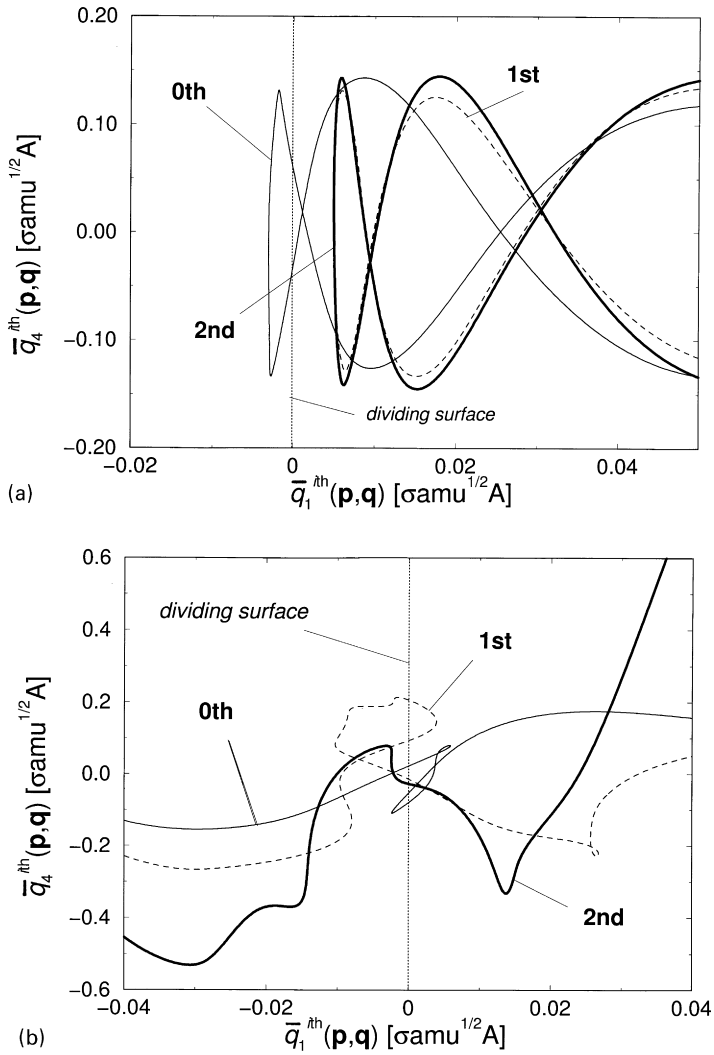

Fig. 5. The projections of the recrossing trajectories onto the zeroth-, first-, and second-order $(\bar{q}_1(\mathbf{p},\mathbf{q}), \bar{q}_4(\mathbf{p},\mathbf{q}))$ plane (a) at 0.05ϵ in Fig. 2 and (b) at 0.5ϵ in Fig. 3.

LCPT. This is because decoupling the motion along the reactive LCPT coordinate removes all forces that would return the system back across the dividing surface. Such nonreactive trajectories are those with insufficient incident momentum in the reactive coordinate $\bar{p}_1(\mathbf{p}(0),\mathbf{q}(0))$ to climb over the saddle.

Next, turn to the behavior of the reactive recrossing trajectory at 0.5ϵ, at which the transition state is almost chaotic (see Fig. 3). Here, as seen in Fig. 5b, the recrossings that occur over the naive dividing surface $S(q_1 = 0)$ in zeroth-order are eliminated; they occur as no-return crossing motions over the second-order dividing surface $S(\bar{q}_1^{2\mathrm{nd}}(\mathbf{p},\mathbf{q}) = 0)$. Furthermore, the system's trajectories along the second-order reactive coordinate $\bar{q}_1^{2\mathrm{nd}}$ are not forced to return to the dividing surface $S(\bar{q}_1^{2\mathrm{nd}} = 0)$ over the (saddle) region, $-0.04 < \bar{q}_1^{2\mathrm{nd}} < 0.04$. On the other hand, the zeroth- and first-order LCPT coordinates are not decoupled from the other modes in the regions either near or more distant from the dividing surface. The second-order LCPT coordinate systems are effectively decoupled to rotate away the apparent

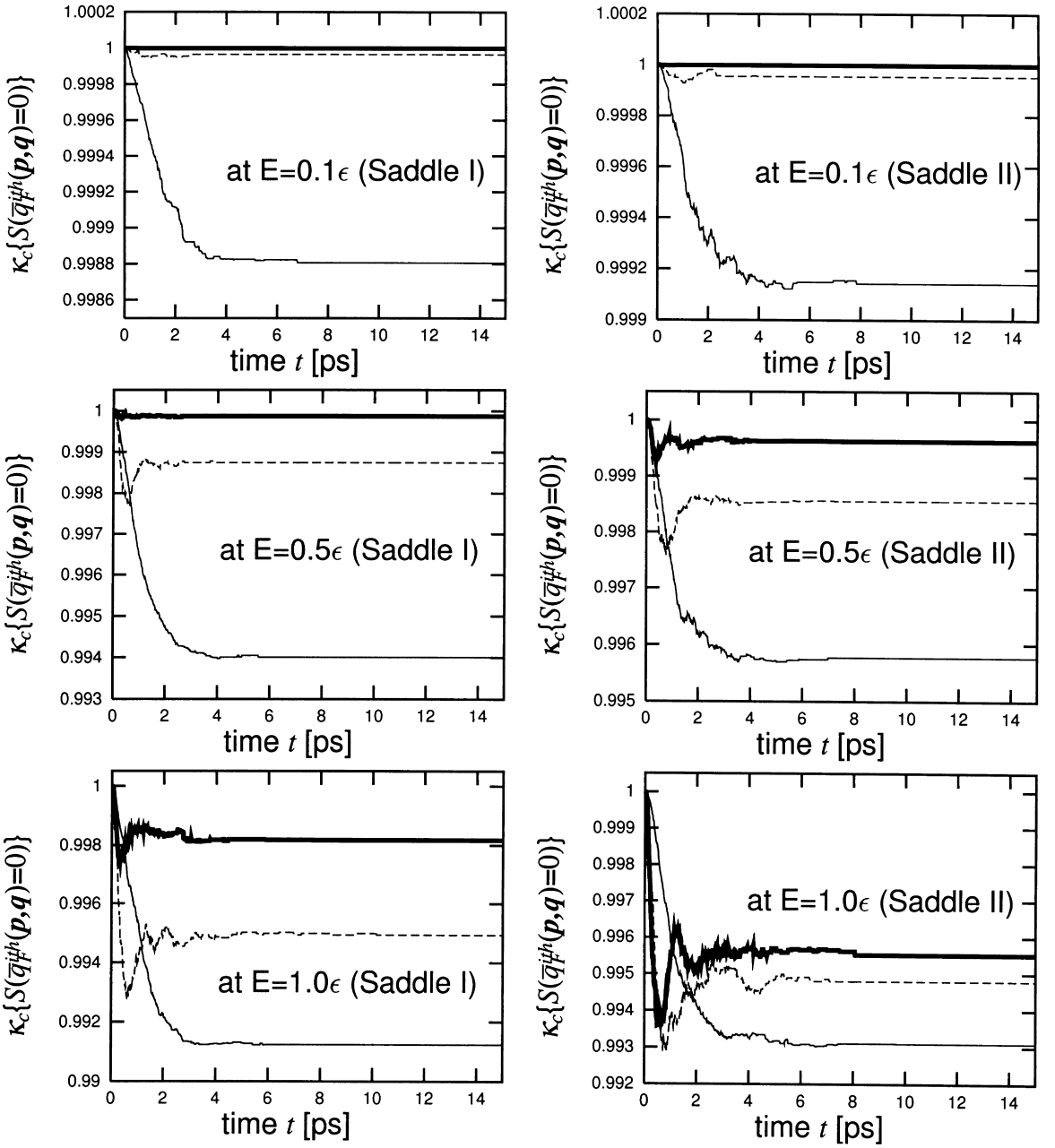

Fig. 6. The transmission coefficient $\kappa_c^{\mathrm{MD}}(t; S(\bar{q}_1^{i\mathrm{th}}(\mathbf{p},\mathbf{q})=0))$ $(i=0,1,2)$ at $E=0.1$, 0.5, and 1.0ϵ for saddle I and saddle II. The solid, dashed, and bold-solid lines denote $\kappa_c^{\mathrm{MD}}(t; S(\bar{q}_1^{i\mathrm{th}}(\mathbf{p},\mathbf{q})=0))$ in terms of the zeroth, first, and second order dividing surface, respectively. For saddle I, the convergent values are 0.9988(0), 0.99996(1), 1.00000(2) (at $E=0.1\epsilon$); 0.9940(0), 0.9987(1), 0.9999(2) (at $E=0.5\epsilon$); 0.9912(0), 0.9949(1), 0.9982(2) (at $E=1.0\epsilon$). For saddle II, 0.9991(0), 0.99995(1), 1.00000(2) (at $E=0.1\epsilon$); 0.9958(0), 0.9986(1), 0.9996(2) (at $E=0.5\epsilon$); 0.9931(0), 0.9948(1), 0.9955(2) (at $E=1.0\epsilon$). The number in the parentheses is the order of the LCPT.

recrossings of the zeroth-order $S(q_1 = 0)$ to the single crossing motion over the LCPT dividing surface $S(\bar{q}_1^{2\text{nd}} = 0)$.

4.3. New transition state rate theory in terms of phase-space dividing hypersurface

It is quite naturally led from the above consequence to reformulate transition state theory in terms of the phase-space dividing surface $S(\bar{q}_1^{2\text{nd}} = 0)$, instead of the conventional configurational dividing surface $S(q_1 = 0)$. The reformulated microcanonical (classical) TST rate constant $\bar{k}^{\text{TST}}$ is obtained as a microcanonical average of the one-way fluxes $j_+(= \dot{\bar{q}}_F(\mathbf{p},\mathbf{q})h(\dot{\bar{q}}_F(\mathbf{p},\mathbf{q})))$ across $S(\bar{q}_F = 0)$ over microcanonical ensembles constructed over a range of energies E.

$$\bar{k}^{\text{TST}}(E) = \langle j_+ \rangle_E = \langle \dot{\bar{q}}_F(\mathbf{p},\mathbf{q})\delta[\bar{q}_F(\mathbf{p},\mathbf{q})]h[\dot{\bar{q}}_F(\mathbf{p},\mathbf{q})]\rangle_E$$
$$= \int_1 \mathrm{d}q_1\, \mathrm{d}p_1 \cdots \int_M \mathrm{d}q_M\, \mathrm{d}p_M$$
$$\times \delta[E - H(\mathbf{p},\mathbf{q})]\dot{\bar{q}}_F(\mathbf{p},\mathbf{q})\delta[\bar{q}_F(\mathbf{p},\mathbf{q})]h[\dot{\bar{q}}_F(\mathbf{p},\mathbf{q})] \tag{17}$$

where $h(x)$ and $\delta(x)$, respectively, denote the Heaviside function and Dirac's delta function of x, and M is the number of DOF. The deviation of $\bar{k}^{\text{TST}}(E)$ from the (classically) exact reaction rate constant $k(E)$, defined as a new transmission coefficient $\kappa_c(= k/\bar{k}^{\text{TST}})$ measures the extent to which a "real" recrossing effect emerges, i.e. *fully developed* chaos in which no invariant of motion exists (if the vibrational energy relaxation is fast enough to let us assume quasi-equilibration in the reactant well). The recipe of calculating the κ_c in terms of $S(\bar{q}_1^{i\text{th}} = 0)$ $(i = 1, 2)$ by using our MD trajectories, $\kappa_c^{\text{MD}}(t; S(\bar{q}_1^{i\text{th}} = 0))$, was given previously [29,41].

Let us now examine $\kappa_c^{\text{MD}}(t; S(\bar{q}_1^{i\text{th}} = 0))$ $(i = 1, 2)$, to see how it behaves with an increase of total energy. Fig. 6 shows those at the three different energies, 0.1, 0.5, 1.0ϵ, above each saddle point energy for saddle I and saddle II, respectively. The zeroth-order estimate $\kappa_c^{\text{MD}}(t; S(\bar{q}_1^{0\text{th}} = 0))$ corresponds to the conventional MD transmission coefficient $\kappa^{\text{MD}}(t)$ based on $S(q_1 = 0)$. The zeroth-order $\kappa^{\text{MD}}(t)$ deviates significantly from unity (except at a very short times) and these deviations increase with increasing total energy. The plateau in $\kappa^{\text{MD}}(t)$ apparent in the figures implies that the recrossing trajectories eventually go into their final state and never again cross the given dividing surface within some interval long compared with the transit time (but obviously still short compared with the time required to establish ergodicity). This plateau value may be identified as the conventional transmission coefficient κ. All these κs smaller for saddle I than for saddle II show that the traditional reaction coordinate q_1 is more coupled to the other bath DOF q_k $(k \neq 1)$ in the region of saddle I than it is near saddle II [15,16,19].

In terms of properties of the phase-space dividing surface, we now show for both the saddles that for low and moderately high energies, the higher is the order of the perturbative calculation, the closer the $\kappa_c^{\text{MD}}(t; S(\bar{q}_1^{i\text{th}} = 0))$ is to unity. Even at energies $\sim 0.5\epsilon$, the plateau values of $\kappa_c(S(\bar{q}_1^{2\text{nd}} = 0))$ are almost unity, e.g. 0.9999 (for saddle I) and 0.9996 (for saddle II). As the total energy becomes much higher, converged values of $\kappa_c(S(\bar{q}_1^{2\text{nd}} = 0))$ deviate significantly from unity (see Fig. 6 at $E = 1.0\epsilon$). We interpret this deviation from unity as the limitation of evaluating the approximate invariants of motion associated with $\bar{q}_1$ with only a few orders of perturbation. At second order, the crossing dynamics over saddle I should exhibit better approximate invariants of motion with $\bar{q}_1$ than that over saddle II because the deviation is smaller for saddle I than that for saddle II. Our result implies that, even in the region where the system is almost chaotic, an approximate analytical expression for (first-rank) saddle-crossing dynamics may nonetheless exist along a negatively curved coordinate in the $(\bar{\mathbf{p}}, \bar{\mathbf{q}})$ space:

$$\frac{\mathrm{d}^2\bar{q}_1^{2\text{nd}}(\mathbf{p},\mathbf{q})}{\mathrm{d}t^2} + (\bar{\omega}_1^{2\text{nd}})^2\bar{q}_1^{2\text{nd}}(\mathbf{p},\mathbf{q}) \simeq 0 \tag{18}$$

4.4. Visualization of phase-space reaction bottleneck

The dividing surface in this representation is analogous to the conventional dividing surface in the sense that it is the point set for which the reaction coordinate has the constant value it has at the saddle-point singularity. However the nonlinear, full-phase-space character of the transformation makes the new crossing surface a complicated, abstract object. We visualize the $S(\bar{q}_1 = 0)$ by projections into spaces of a few

Table 1
The number of non-reactive (n, n, σ) crossings in 10,000 well–saddle–well trajectories across the $S(q_1 = 0)$ and the decompositions into those over the ith order phase-space dividing surface $S(\bar{q}_1^{\text{ith}}(\mathbf{p}, \mathbf{q}) = 0)$ $(i = 1, 2)$ for saddle I at $E = 0.1$, and 0.5ϵ

$S(q_1 = 0)$	1st order					2nd order			
	$0 = n$	1	2	3	5	$n = 0$	1	2	3
$E = 0.1\epsilon$									
26(1,1,+)	23(0,0,+)	3(1,1,+)				26(0,0,+)			
1(2,2,+)	1(0,0,+)					1(0,0,+)			
161(1,1,−)	160(0,0,−)		1(2,2,−)			161(0,0,−)			
7(2,2,−)	5(0,0,−)	1(1,1,−)	1(2,2,−)			7(0,0,−)			
$E = 0.5\epsilon$									
67(1,1,+)	50(0,0,+)	15(1,1,+)	1(2,2,+)	1(3,3,+)		63(0,0,+)	4(1,1,+)		
6(2,2,+)	4(0,0,+)	2(1,1,+)				6(0,0,+)			
1(4,4,+)					1(5,5,+)			1(2,2,+)	
329(1,1,−)	303(0,0,−)	24(1,1,−)	2(2,2,−)			327(0,0,−)	1(1,1,−)	1(2,2,−)	
23(2,2,−)	14(0,0,−)	6(1,1,−)	2(2,2,−)	1(3,3,−)		20(0,0,−)		2(2,2,−)	1(3,3,−)
1(3,3,−)	1(0,0,−)					1(0,0,−)			

dimensions, e.g., the (q_j, q_k) plane:

$$\bar{S}(q_j, q_k; E) = \langle \delta[\bar{q}_F(\mathbf{p}', \mathbf{q}')]\delta(q_j' - q_j)\delta(q_k' - q_k)\rangle_E$$
$$= \int_1 \mathrm{d}q_1' \, \mathrm{d}p_1' \cdots \int_M \mathrm{d}q_M' \, \mathrm{d}p_M'$$
$$\times \delta[E - H(\mathbf{p}', \mathbf{q}')]\delta[\bar{q}_F(\mathbf{p}', \mathbf{q}')]$$
$$\times \delta(q_j' - q_j)\delta(q_k' - q_k) \qquad (19)$$

In this paper, we show the (q_1, q_2) projections for the crossings over the lowest saddle, saddle I. The projection onto the q_1 is an important device to reveal how the $S(\bar{q}_1 = 0)$ differs from the conventional dividing surface $S(q_1 = 0)$. (Remember that in an energy range close to the threshold energy in which the normal mode picture is approximately valid, the phase space $S(\bar{q}_1 = 0)$ collapses onto the traditional configuration-space surface where $q_1 = 0$). The computational recipe was given previously [30].

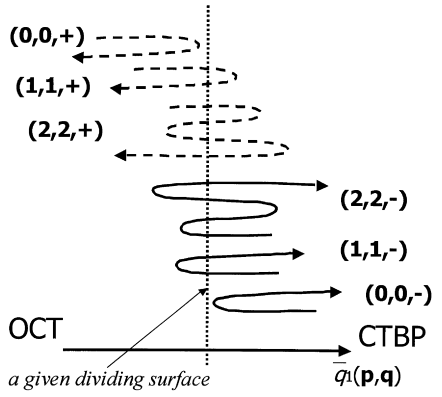

Fig. 7. The schematic pictures of the (0,0, +), (0,0, −), (1,1, +), (1,1, −), (2,2, +), and (2,2, −) crossings at saddle I.

To do this, first let us look into the complicated non-reactive, recrossing behavior of trajectories over the conventional dividing surface $S(q_1 = 0)$ at saddle I. Table 1 shows the numbers of non-reactive crossings in 10,000 well–saddle–well trajectories over the $S(q_1 = 0)$ and how these evolve into their counterparts over the phase-space dividing surface $S(\bar{q}_1^{\text{ith}}(\mathbf{p}, \mathbf{q}) = 0)$ as the energy increases from $E = 0.1$ to 0.5ϵ. Here (N_{+-}, N_{-+}, σ) represents the number of times each crosses the dividing surface in a specific direction: if a crossing trajectory, whose sign of the flux at the first crossing is σ, crosses a given dividing surface N_{+-} times from positive to negative, and N_{-+} times from negative to positive along the reactive coordinate, the trajectory is classified into the (N_{+-}, N_{-+}, σ)-type crossing, e.g. for saddle I a trajectory which crosses the dividing surface two times and the first crossing is from the OCT to the CTBP minimum is (1,1, +). The $(0,0,\sigma)$ denote non-reactive, *non-crossing* trajectories climbing the saddle from the $-\sigma$ side on the reactive coordinate $\bar{q}_1^{\text{ith}}$ (see Fig. 7).

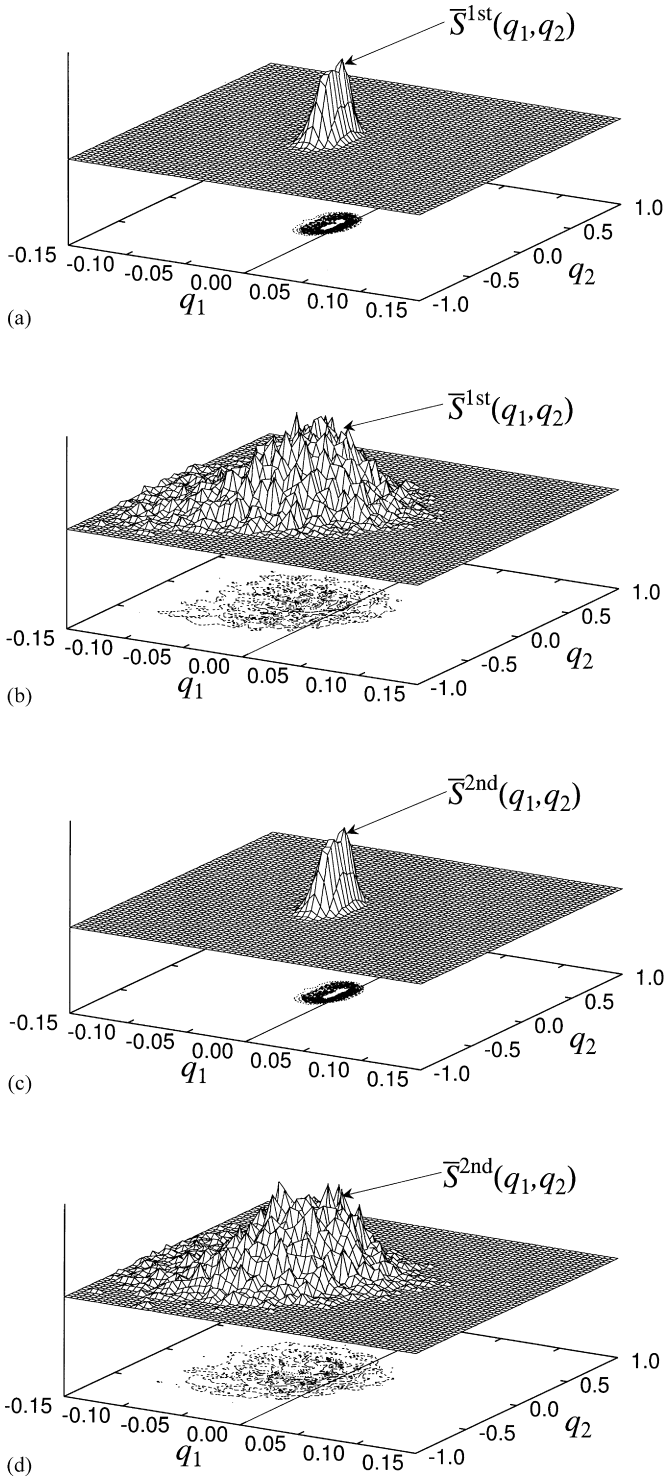

Fig. 8. $\bar{S}^{1st}(q_1,q_2)$ and $\bar{S}^{2nd}(q_1,q_2)$ at saddle I. (a) $E = 0.1\epsilon$, (b) $E = 0.5\epsilon$ for $\bar{S}^{1st}(q_1,q_2)$; (c) $E = 0.1\epsilon$, (d) $E = 0.5\epsilon$ for $\bar{S}^{2nd}(q_1,q_2)$.

The table tells us the trajectories climbing from the second CTBP minimum are more likely to return after crossing $S(q_1 = 0)$, than the trajectories from the OCT global minimum (see the first column in Table 1. e.g. $161(1,1,-) \gg 26(1,1,+)$ at 0.1ϵ; $329(1,1,-) \gg 67(1,1,+)$ at 0.5ϵ), while the corresponding figures are essentially the same for the symmetrical saddle II within the statistical error [30]. How is each of the (n,n,σ)-saddle crossings over the $S(q_1 = 0)$ transformed into its counterpart over the phase-space dividing surface $S(\bar{q}_1^{i\text{th}}(\mathbf{p},\mathbf{q}) = 0)$? At 0.1ϵ, all non-reactive recrossing trajectories observed over the $S(q_1 = 0)$ are rotated away into non-reactive, non-crossing trajectories, and all reactive recrossings over the $S(q_1 = 0)$ into reactive single crossings, maintaining their directionality of the saddle crossing, over the second-order dividing surface $S(\bar{q}_1^{2\text{nd}}(\mathbf{p},\mathbf{q}) = 0)$. The first-order $S(\bar{q}_1^{1\text{st}}(\mathbf{p},\mathbf{q}) = 0)$ leaves some recrossings because it only incompletely decouples the reactive coordinate from the others. The higher the total energy, ca. 0.5ϵ, the more recrossings remain even at second-order LCPT; nevertheless the directionality of their saddle crossings is preserved. Note that the degrees of incomplete transformation of non-reactive recrossing trajectories (n,n,σ) over $S(q_1 = 0)$ into non-reactive non-crossings seem to differ distinctly in different directions of climbing. For example, in first order at 0.5ϵ, the (1,1,−) crossings are transformed 303/329 ≃ 92% to the (0,0,−) while the (1,1,+) crossings are transformed only 50/67 ≃ 75%. (These are essentially equal within the statistical error for saddle II, as they should be for its symmetrical character [30].)

While so far there have been no means to address why, on passing through the transition state, there is such a distinct dependence in probability on the direction of climbing, we can now probe deeper into such questions by visualizing our phase-space dividing surface. (The naive picture, based simply on the height of the barrier to reaction as an exponential factor in the rate, remains valid, of course.) Fig. 8 shows projections of the ith order dividing surface $S(\bar{q}_1^{i\text{th}}(\mathbf{p},\mathbf{q}) = 0)$ onto the two-dimensional (q_1, q_2) subspace for saddle I at $E = 0.1$, and 0.5ϵ. As the total energy increases, the projections of the phase-space dividing surfaces, $S(\bar{q}_1^{i\text{th}}(\mathbf{p},\mathbf{q}) = 0)$ $(i = 1, 2)$, broaden and extend to regions more removed from the conventional dividing surface $S(q_1 = 0)$. Note that these $S(\bar{q}_1(\mathbf{p},\mathbf{q}) = 0)$ are more heavily distributed on the minus side (to the OCT minimum) than on the plus side (to the CTBP minimum) in q_1. This asymmetrical feature of the $S(\bar{q}_1(\mathbf{p},\mathbf{q}) = 0)$ explains the higher frequencies found for $(n,n,-)$- than for $(n,n,+)$-type crossings over $S(q_1 = 0)$. Namely, if the *real* dividing surface $S(\bar{q}_1(\mathbf{p},\mathbf{q}) = 0)$ is mainly distributed on the minus side in q_1, and the system once crossed the *naive* dividing surface $S(q_1 = 0)$ from minus to plus, the system rarely returns to the $S(q_1 = 0)$ because of the small driving force to make the system go back to $S(q_1 = 0)$ after it has passed the greater part of the distribution constituting the real $S(\bar{q}_1 = 0)$. In the same way, even if the system crossed the $S(q_1 = 0)$ from plus to minus, the system has not necessarily passed the surface $S(\bar{q}_1) = 0$. The system will recross the $S(q_1 = 0)$ if the system does not possess sufficient incident (reactive) momentum $\bar{p}_1$ to pass through the $S(\bar{q}_1 = 0)$. The ease of transforming $(n,n,-)$ to (0,0,−) compared with $(n,n,+)$ to (0,0,+) for saddle I may arise from this asymmetrical nature of $S(\bar{q}_1(\mathbf{p},\mathbf{q}) = 0)$; almost non-reactive recrossings initiated from the CTBP state occur because the *real* dividing surface mainly distributes outwards to the OCT side from the $S(q_1 = 0)$, while the less frequent non-reactive recrossings from the other OCT state occur when the system finds an edge of the reaction bottleneck, i.e. a tiny part of the dividing hypersurface in the phase space. In other words, the outward migration of $S(\bar{q}_1(\mathbf{p},\mathbf{q}) = 0)$ can be taken into account efficiently by a few low orders of LCPT (e.g. first-order at 0.5ϵ), but higher-order LCPT calculations would be crucial to establish such a edge of the reaction bottleneck in these high energies, e.g. second-order at 0.5ϵ.

We also found [30] that besides total energy the velocity across the transition state plays a major role in many-DOF systems to move the reaction bottleneck outwards from the naive dividing surface $S(q_1 = 0)$. A similar picture has been observed by Pechukas et al. [42–44] in two-dimensional Hamiltonian systems, e.g. collinear H + H_2, H + Cl_2, and F + H_2 reactions, by using a so-called periodic orbit dividing surface (PODS) theory. Their crucial idea is based on the findings of periodic orbits in the saddle region. In many M-dimensional systems $(M > 2)$, the saddle-crossing dynamics often behave chaotically due to resonances among the stable bath-DOF,

blowing out (M-dimensional) periodic orbits in the transition state. As far as we know, this is the first example to picture reaction bottlenecks for such many-DOF systems.

Although Fig. 8 revealed the origin of the ease of climbing the saddle depending on the direction of reaction, it also indicates the limit of our present method to picture the phase-space dividing surfaces. The projected ith order phase-space dividing surfaces onto the (q_1, q_2) plane are almost indistinguishable for both the orders, $\bar{S}^{1st}(q_1, q_2)$ and $\bar{S}^{2nd}(q_1, q_2)$. However, as apparently seen in Figs. 5 and 6, the second order is essential to extract an invariant of motion along the reactive degrees of freedom $\bar{q}_1$ from the many-DOF phase space, which rotates away the apparent recrossings observed over the naive $S(q_1 = 0)$, while the zeroth-, and first-order are not. First, would it be possible to fully picture or imagine the nonlinear, full-phase-space character of such a dividing hypersurface? The question related to this is: "How can the full dimension of the system be reduced to a lower dimensionality, just enough to represent the essence of many-dimensional saddle crossing dynamics?" We are now analyzing this [45] in terms of principal component or coordinate analysis [46] recently introduced for dynamical problems in proteins [47,48].

One further point will clarify how the separability of even the reactive degree of freedom disappears at high energies. With increasing energy, the *length* of the path where the reactive mode is separable decreases. The region of nonlinear coupling and mode-mode mixing encroaches closer and closer to the saddle point as the energy of the system grows. At sufficiently high energies, the length of the separable region is so small that the system traverses it in only a few vibrational periods, or even only a fraction of a cycle. In this case, regularity, separability and preservation of local approximate constants of motion lose their meaning, and one must say that even the reactive mode is chaotic.

5. Conclusions

We showed that in the reactive degree of freedom obtained by transformation with Lie canonical perturbation theory, separability and regular behavior persists, yielding unit transmission coefficients, up to moderately high energies, even when all other degrees of freedom are chaotic. We also presented one possible way to visualize the phase-space reaction bottleneck by the projections of this hypersurface onto low-dimensional subspaces. Such projections clarify how the system traverses the configurational dividing surface $S(q_1 = 0)$. The essence of our findings is the demonstration of the existence of at least one approximate invariant of motion which survives in the transition state region, and is specifically associated with the reactive coordinate $\bar{q}_F(\mathbf{p}, \mathbf{q})$. This is because the small-denominator problem never happens if the frequency of one mode is imaginary and the rest are real; the reactive mode in the present case is the one in the combination with an imaginary frequency. The other frequencies associated with bath modes fall on the real axis, orthogonal to the imaginary axis in the complex ω-plane. That is

$$\left|\sum_{k=1}^{3N-6}{}^{\dagger} n_k \omega_k\right| \geq |\omega_F| > \mathrm{O}(\epsilon^n) \tag{20}$$

for arbitrary integers n_k with $n_F \neq 0$, where $\sum^{\dagger}$ denotes the combination including the reactive mode. This was first pointed out by Hernandez and Miller [49–51].[1] Thus, this feature is quite generic in the region of (first-rank) transition states, irrespective of the system we consider. In terms of regularity of the dynamics there are three distinct levels of local dynamics in the transition state: quasi-regular, semi-chaotic, and fully-developed chaotic regions [29,30].

In the lowest reaches of the energy above the saddle, as in Fig. 2, all or almost all the degrees of freedom of the system *locally* maintain approximate constants of motion in the region of the transition state. We identify such a range of energy, in which the rate coefficient shows staircase structure [24–26] as corresponding to this quasi-regular region. As shown in Fig. 3, with increasing energy, *almost* all of the approximate invariants of motion disappear, inducing a topological change in dynamics from quasi-regular to chaotic in the regions of transition states. However at least one approximate invariant

[1] The transformation of $(\mathbf{p}, \mathbf{q})$ to action-angle variables in the transition state was first studied in semi-classical TST theories.

of motion survives during the saddle crossings, that associated with the reactive coordinate $\bar{q}_1(\mathbf{p},\mathbf{q})$. This intermediate, semi-chaotic region, does not exist near potential minima, but is inherently associated with (first-rank) transition states. In both quasiregular and semi-chaotic regions, the well-defined phase-space dividing surface can be extracted, across which the long-standing ambiguity of transition state theories, recrossing problem, can be rotated away giving unit transmission coefficients. As total energy becomes much higher, the system becomes subject to considerable nonlinearities of the potential energy surface, and a few orders of perturbation theory are not adequate to eliminate the recrossings. In this paper, we analyzed LCPT up to a (finite) second-order, where no commensurable conditions were encountered at these orders. While it is not apparent how far a region of regularity would extend in higher orders, even if an infinite, or sufficiently higher-order perturbation calculation would be performed, the convergence radius becomes negligibly small near the unstable saddle point for the invariant of motion with $\bar{q}_1$. In this energy region, the saddle-crossing dynamics encroaches so closely on the saddle point that only an infinitesimal region of regularity remains and is entirely stochastic.

The recrossing effect has been one of the big ambiguities in the transition state theories and has been often dealt with by Kramers–Grote–Hynes [4,5] theories. van der Zwan and Hynes [52] proved that, for a class of Hamiltonians representing of parabolic barrier–harmonic oscillator systems linearly coupled with stable bath modes, transition state theory is equivalent to the Grote–Hynes formulation with the parabolic mode as the reactive degree of freedom, if the reaction coordinate is chosen as an unstable normal coordinate composed of the total system (= reaction system + bath). Our results indicate that their equivalence should be much more general and apply to a wider range of Hamiltonian classes, even when the system is almost chaotic.

The remaining ambiguity common in both the transition state theories and the Kramers–Grote–Hynes theories (in the high-viscosity region) is the quasi-equilibrium assumption in the well of the reactants: the reaction system moves about ergodically in all possible phase space reactant domains before crossing the transition state. One possible diagnostic tool to look deeper into this question in many-degrees-of-freedom systems would be to follow the backward trajectory starting on the phase-space dividing hypersurface $S(\bar{q}_1(\mathbf{p},\mathbf{q})=0)$, sampled from the microcanonical ensemble. If the microcanonical backward trajectories would only move about in a certain limited phase space in the reactant domain, it should show how the quasi-equilibrium assumption is violated before the crossings of the transition state occur. The backward calculations having large momenta $\bar{p}_1(\mathbf{p},\mathbf{q})$ on that hypersurface would reveal how the mode-specific nature of reactions relates to the local topography of the phase space in the reactant state. Related to this, the correlations among the successive saddle crossings occurring in dynamic relaxation on rugged potential energy surfaces (PESs) can be elucidated in terms of such backward trajectories from $S(\bar{q}_1(\mathbf{p},\mathbf{q})=0)$ at one transition state and the forward trajectories from the other $S(\bar{q}_1(\mathbf{p},\mathbf{q})=0)$ at the previous transition state, through which the system has passed before the first one [53]. While through this paper we dealt with the first-rank transition states, especially in the cases of the relaxation dynamics, the system trajectories may pass over higher-rank saddles of the PES. These provides us with a new, untouched, exciting problem, i.e. what is the role of resonance in the imaginary ω-plane for the bifurcation? With this, we encounter the many related open subjects incorporated into statistical theories of many-DOF systems.

Acknowledgements

We thank Prof. S.A. Rice, Prof. R.T. Skodje, Dr M. Toda, and Prof. J.A.W. Brickmann for their insightful discussions and valuable comments. This study was supported by a grant from the National Science Foundation.

References

[1] S. Glasstone, K.J. Laidler, H. Eyring, The Theory of Rate Processes, McGraw-Hill, New York, 1941.
[2] J.C. Keck, Adv. Chem. Phys. 13 (1967) 85.
[3] D.G. Truhlar, B.C. Garrett, Acc. Chem. Res. 13 (1980) 440.
[4] J.T. Hynes, in: M. Baer (Ed.), Theory of Chemical Reaction Dynamics, CRC Press, Boca Raton, FL, 1985, pp. 171–234.
[5] H.A. Kramers, Physica 7 (1940) 284.

[6] B.J. Berne, M. Borkovec, J.E. Straub, J. Phys. Chem. 92 (1988) 3711.
[7] D.G. Truhlar, B.C. Garrett, S.J. Kippenstein, J. Phys. Chem. 100 (1996) 12771.
[8] D.C. Chatfield, R.S. Friedman, S.L. Mielke, G.C. Lynch, T.C. Allison, D.G. Truhlar, D.W. Schwenke, in: R.E. Wyatt, J.Z.H. Zhang (Eds.), Dynamics of Molecules and Chemical Reactions, Marcel Dekker, New York, 1996, p. 323.
[9] M.J. Davis, S.K. Gray, J. Chem. Phys. 84 (1986) 5389.
[10] S. Wiggins, Normally Hyperbolic Invariant Manifolds in Dynamical Systems, Springer, New York, 1991.
[11] R.E. Gillian, G.S. Ezra, J. Chem. Phys. 94 (1991) 2648.
[12] M. Toda, Phys. Rev. Lett. 74 (1995) 2670.
[13] M. Toda, Phys. Lett. A 227 (1997) 232.
[14] T.L. Beck, D.M. Leitner, R.S. Berry, J. Chem. Phys. 89 (1988) 1681.
[15] D.J. Wales, R.S. Berry, J. Phys. B 24 (1991) L351.
[16] R.J. Hinde, R.S. Berry, D.J. Wales, J. Chem. Phys. 96 (1992) 1376.
[17] C. Amitrano, R.S. Berry, Phys. Rev. Lett. 68 (1992) 729.
[18] C. Amitrano, R.S. Berry, Phys. Rev. E 47 (1993) 3158.
[19] R.J. Hinde, R.S. Berry, J. Chem. Phys. 99 (1993) 2942.
[20] R.S. Berry, Chem. Rev. 93 (1993) 237.
[21] R.S. Berry, Int. J. Quantum Chem. 58 (1996) 657.
[22] K. Ball, R.S. Berry, R.E. Kunz, F.-Y. Li, A. Proykova, D.J. Wales, Science 271 (1996) 963.
[23] S.K. Nayak, P. Jena, K.D. Ball, R.S. Berry, J. Chem. Phys. 108 (1998) 234.
[24] E.R. Lovejoy, S.K. Kim, C.B. Moore, Science 256 (1992) 1541.
[25] E.R. Lovejoy, C.B. Moore, J. Chem. Phys. 98 (1993) 7846.
[26] S.K. Kim, E.R. Lovejoy, C.B. Moore, J. Chem. Phys. 102 (1995) 3202.
[27] T. Komatsuzaki, M. Nagaoka, J. Chem. Phys. 105 (1996) 10838.
[28] T. Komatsuzaki, M. Nagaoka, Chem. Phys. Lett. 265 (1997) 91.
[29] T. Komatsuzaki, R.S. Berry, J. Chem. Phys. 110 (1999) 9160.
[30] T. Komatsuzaki, R.S. Berry, Phys. Chem. Chem. Phys. 1 (1999) 1387.
[31] A.J. Lichtenberg, M.A. Lieberman, Regular and Chaotic Dynamics, 2nd ed., Springer, New York, 1992.
[32] J.R. Cary, Phys. Rep. 79 (1981) 130.
[33] L.E. Fried, G.S. Ezra, J. Chem. Phys. 86 (1987) 6270.
[34] L.E. Fried, G.S. Ezra, Comp. Phys. Commun. 51 (1988) 103.
[35] L.E. Fried, G.S. Ezra, J. Phys. Chem. 92 (1988) 3144.
[36] M. Page, J.W. McIver Jr., J. Chem. Phys. 88 (1988) 922.
[37] D.C. Chatfield, R.S. Friedman, D.G. Truhlar, B.C. Garrett, D.W. Schwenke, J. Am. Chem. Soc. 113 (1991) 486.
[38] D.C. Chatfield, R.S. Friedman, D.G. Truhlar, D.W. Schwenke, Faraday Discuss. Chem. Soc. 91 (1991) 289.
[39] D.C. Chatfield, R.S. Friedman, G.C. Lynch, D.G. Truhlar, D.W. Schwenke, J. Chem. Phys. 98 (1993) 342.
[40] W.H. Press, S.A. Teukolsky, W.T. Vetterling, B.P. Flannery, Numerical Recipes, 2nd ed., Cambridge University Press, New York, 1992.
[41] J.P. Bergsma, J.R. Reimers, K.R. Wilson, J.T. Hynes, J. Chem. Phys. 85 (1986) 5625.
[42] P. Pechukas, E. Pollak, J. Chem. Phys. 67 (1977) 5976.
[43] E. Pollak, in: D.C. Clary (Ed.), Theory of Chemical Reaction Dynamics, NATO ASI Series, C 170, Reidel, Dordrecht, 1985, p. 135.
[44] E. Pollak, in: M. Baer (Ed.), Theory of Chemical Reaction Dynamics, CRC Press, Boca Raton, FL, 1986, p. 123.
[45] T. Komatsuzaki, R.S. Berry, unpublished.
[46] J.C. Gower, Biometrica 55 (1968) 582.
[47] O. Becker, M. Karplus, J. Chem. Phys. 106 (1997) 1495.
[48] N. Elmaci, R.S. Berry, J. Chem. Phys. 110 (1999) 10606.
[49] R. Hernandez, W.H. Miller, Chem. Phys. Lett. 214 (1993) 129.
[50] W.H. Miller, Faraday Discuss. Chem. Soc. 62 (1977) 40.
[51] T. Seideman, W.H. Miller, J. Chem. Phys. 95 (1991) 1768.
[52] G. van der Zwan, J.T. Hynes, J. Chem. Phys. 78 (1983) 4174.
[53] T. Komatsuzaki, M. Toda, S.A. Rice, R.S. Berry, unpublished.